International Journal of Bioprinting

RESEARCH ARTICLE

Bioprinting of hydrogel beads to engineer pancreatic tumor-stroma microtissues for drug screening

Beisi Huang[1†], Xiaoyun Wei[1†*], Keke Chen[1], Ling Wang[1,2*], Mingen Xu[1,2*]

[1]School of Automation, Hangzhou Dianzi University, Hangzhou 310018, China

[2]Key Laboratory of Medical Information and 3D Bioprinting of Zhejiang Province, Hangzhou Dianzi University, Hangzhou 310018, China

(This article belongs to the *Special Issue: Advances in 3D bioprinting for regenerative medicine and drug screening*)

Abstract

Pancreatic ductal adenocarcinoma (PDAC) having features of dense fibrotic stromal and extracellular matrix (ECM) components has poor clinical outcome. *In vitro* construction of relevant preclinical PDAC models recapitulating the tumor-stroma characteristics is therefore in great need for the development of pancreatic cancer therapy. In this work, a three-dimensional (3D) heterogeneous PDAC microtissue based on a dot extrusion printing (DEP) system is reported. Gelatin methacryloyl (GelMA) hydrogel beads encapsulating human pancreatic cancer cells and stromal fibroblasts were printed, which demonstrated the capacity of providing ECM-mimetic microenvironments and thus mimicked the native cell-cell junctions and cell-ECM interactions. Besides, the spherical structure of the generated hydrogel beads, which took the advantage of encapsulating cells in a reduced volume, enabled efficient diffusion of oxygen, nutrients and cell waste, thus allowing the embedded cells to proliferate and eventually form a dense pancreatic tumor-stroma microtissue around hundred microns. Furthermore, a tunable stromal microenvironment was easily achieved by adjusting the density of stromal cells in the hydrogel beads. Based on our results, the produced heterogeneous pancreatic microtissue recapitulated the features of cellular interactions and stromal-like microenvironments, and displayed better anti-cancer drug resistance than mono-cultured pancreatic cancer spheroids. Together, the DEP system possesses the ability to simply and flexibly produce GelMA hydrogel beads, providing a robust manufacturing tool for the pancreatic cancer drug screening platform fabrication. In addition, the engineered pancreatic tumor-stroma microtissue based on bioprinted GelMA hydrogel beads, other than being ECM-biomimetic and stroma-tunable, can be used for observation *in situ* and may serve as a new drug screening platform.

Keywords: 3D bioprinting; GelMA hydrogel beads; Tumor-stroma microtissues; Tunable stromal microenvironment; Drug screening

†These authors contributed equally to this work.

***Corresponding authors:**
Xiaoyun Wei
(wxyun@hdu.edu.cn)
Ling Wang
(lingw@hdu.edu.cn)
Mingen Xu
(xumingen@hdu.edu.cn)

Citation: Huang B, Wei X, Chen K, *et al*., 2023, Bioprinting of hydrogel beads to engineer pancreatic tumor-stroma microtissues for drug screening. *Int J Bioprint,* 9(3): 676. https://doi.org/10.18063/ijb.676

Received: August 31, 2022

Accepted: November 22, 2022

Published Online: February 01, 2023

Copyright: © 2023 Author(s). This is an Open Access article distributed under the terms of the Creative Commons Attribution License, permitting distribution, and reproduction in any medium, provided the original work is properly cited.

Publisher's Note: Whioce Publishing remains neutral with regard to jurisdictional claims in published maps and institutional affiliations.

1. Introduction

Pancreatic ductal adenocarcinoma (PDAC) is a highly aggressive malignancy with an escalating trend of mortality rate[1,2]. As reported, PDAC progresses rapidly and has a

5-year survival rate of <8%[3]. PDAC, which has a complex surrounding anatomical structure, is hidden in the human body. Most of the patients reach middle and late stage by the time of diagnosis, and the tumor can only be surgically resected in <20% of the patients[4,5]. Drug therapy thus plays a major role in the treatment of PDAC. However, the development outcome of drug therapy for pancreatic cancer is still far from ideal although a gradual increase of research funding's were allocated annually to develop drugs for treating pancreatic cancer. Furthermore, the ineffective drug prediction ability of preclinical PDAC model impedes the development of novel drug treatment[6].

The pancreatic cancer microenvironment is composed of parenchymal cancer cells, diversiform stromal cells, and non-cellular components, such as extracellular matrix (ECM) and cell secreted factors[7-9]. A line of clinical evidence has shown that it is difficult to treat PDAC because of low cure rate and poor prognosis, which are closely related to the unique bioarchitecture of the cancer[10,11]. In the PDAC development process, pancreatic cancer cells promoted a large number of cancer-associated fibroblasts (CAFs) formed by activating the matrix components, mainly pancreatic stellate cells (PSCs), scattered around the acinar follicle. The activated stromal components further contribute to excessive ECM deposition, and eventually lead to pancreatic cancer cells being embedded in a dense fibrous barrier[12-14]. This unique tumor-stroma niche regulates complex crosstalk between pancreatic cancer cells and CAFs, and further promotes the progression and drug resistance of pancreatic cancer cells[15,16]. Therefore, building *in vitro* biomimetic PDAC models to outline key tumor-stroma features will facilitate the cancer drug development.

Three-dimensional (3D) cultured tumor spheroids provide key structural features of biomimetic *in vivo* solid tumors, including tight cell-cell, cell-ECM physical contactions, similar pH/nutrient/oxygen gradients, and abundant cell communication, as well as exhibit different responses to drugs better than 2D cultured cells, and have been widely used in the screening of anti-tumor drugs in recent years[17-19]. For example, João F. Mano's research group engineered heterogeneous PDAC spheroids to mimic PDAC-stroma features by co-culturing tumor and stromal cells using ultra-low adhesion plate[20]. Recently, they further reported a novel "cancer-on-a-bead" platform which produced hydrogel beads encapsulating tumor and stroma cells by superhydrophobic surfaces[21]. The generated cancer models processing tumor-stroma bioarchitectures and ECM microenvironments had an increased drug resistance performance. However, there were some shortcomings: the limited growth space of ultra-low adhesion plate could not provide a long-term and stable cell growth environment, thereby causing nutrition inadequacy and a lack of gas and waste exchange. On the other hand, the position of hydrogel beads prepared by superhydrophobic array was not fixed, which might cause sample loss and other problems in the subsequent liquid exchange process.

3D bioprinting has great advantages in building complex tissue models using accurately controlled assembly of cells, hydrogels and active molecules to form specific structures[22-24]. Herein, we established stroma-tunable PDAC models by printing cell-laden gelatin methacryloyl (GelMA) hydrogel beads through the dot extrusion printing (DEP). As shown in Figure 1, GelMA hydrogel beads were facile printed and supported pancreatic cancer cells (BxPC-3) and stromal cells to form a dense tumor-stroma microtissue, which reproduced the characteristics of stromal microenvironment and ECM component *in vivo*. The printed GelMA beads were biocompatible and in reduced volume, which are conducive to nutrient uptake by encapsulated cells and waste excretion. In the co-culture session, we observed that tumor spheroids acquired enhanced proliferation and the normal fibroblasts were activated and transformed to CAF phenotype. Further, in the chemotherapeutic drug (gemcitabine) treatment, tumor-stroma PDAC models had a stronger drug resistance when compared with the mono-cultured tumor. The engineered PDAC microtissue with stromal cellular barrier formed in 3D GelMA beads is useful for studying cancer drug resistance and the underlying molecular mechanisms, and it is an effective *in vitro* drug screening platform for pancreatic cancer drug therapy research.

2. Materials and methods

2.1. Cell culture

Human pancreatic cancer cell line (BxPC-3) and normal human dermal fibroblast cells (NHDFs) in this work were kindly provided by Hangzhou Regenovo Biotechnology Co., Ltd. For cells cultivation, BxPC-3 and NHDFs were cultured in RPMI-1640 and Dulbecco's modified Eagle's medium (DMEM; Gibco, USA), respectively. About 10% (v/v) fetal bovine serum (FBS; Excell Bio, China) and 1% (v/v) penicillin/streptomycin (Thermo, USA) were supplemented into the above-mentioned basic medium. Cells were cultured at 37°C under 5% CO_2, and passaged at 3-day intervals.

2.2. Material preparation

GelMA was provided by Hangzhou Regenovo Biotechnology Co., Ltd. The selected concentration of GelMA was 8% (w/v) and the concentration of lithium phenyl-2, 4, 6-trimethylbenzoylphosphinate (LAP; Sigma Aldrich, USA) was 0.5% (w/v). GelMA and photoinitiator

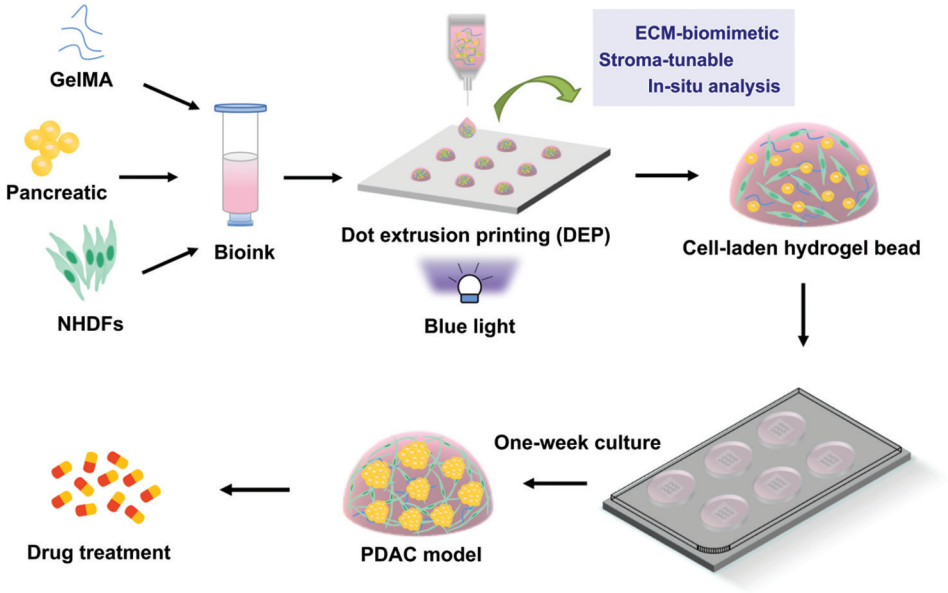

Figure 1. Schematic presentation of this study. Three-dimensional pancreatic ductal adenocarcinoma (PDAC) models were fabricated by bioprinting of pancreatic cancer BxPC-3 cells and normal human dermal fibroblast cells laden-GelMA hydrogel beads using the dot extrusion printing technology. Drug treatment on the uniform-sized PDAC models was conducted after 1-week culture.

LAP were fully dissolved using DMEM as solvent in a 47°C water bath for 1 h. The prepared GelMA solution was fully sterilized by passing it through a 0.22-μm filter, and then stored at 4° for future use.

2.3. Bioprinting system

3D bioprinter (Bio-Architect WS) used in the experiments was provided by Hangzhou Regenovo Biotechnology Co., Ltd. The temperature of the receiving platform and the printhead was independently controlled. The printing path of the printhead can be controlled by inputting G-code into the bioprinter.

To print the array of GelMA hydrogel beads, a pre-set G-code was adopted, which enables the printhead working in an intermittent pressure-driven mode. In this work, printing nozzle with an inner diameter of 0.21 mm was selected to print the GelMA hydrogel beads. To ensure smooth extrusion of the GelMA hydrogel beads, the printing nozzle was calibrated in coordinates before printing, to keep a proper distance between the printing nozzle tip and the receiving platform. To produce GelMA hydrogel beads in different sizes, the driven pressure was fixed at 0.1 MPa, and the dispensing time ranging from 1000 to 1800 ms was tested by setting the value in the G-code.

2.4. GelMA beads morphology and porosity characterization

For studying the inner morphology, the GelMA hydrogel beads were placed at −80°C for 2 h, then lyophilized by freeze dryer. Before characterization, hydrogel samples were immersed in liquid nitrogen for 60 s, and then covered by a thin layer of Au film. Finally, sections of hydrogel were scanned by scanning electron microscopy (SEM; SU-8010, Japan). The porosity analysis of hydrogel beads was then quantified using ImageJ software.

To explore the diffusion ability of the GelMA beads, we prepared the fluorescein isothiocyanate (FITC)-diffusion analysis by immersing the printed hydrogel beads in the medium containing FITC (100 μg/mL). Fluorescent images were obtained at 0, 10 and 20 min using the fluorescence microscope.

2.5. PDAC microtissues bioprinting

BxPC-3 cells were fully mixed with the prepared GelMA solution at a cell concentration of 3×10^6 cells/mL to obtain the bioink for homogeneous microtissue printing. To fabricate the stroma-tunable PDAC microtissues, BxPC-3 cells and NHDFs with different cell densities were printed. Specifically, BxPC-3 cells and NHDFs at the concentration of 3×10^6 cells/mL and 6×10^6 cells/mL (1:2), respectively, were mixed with GelMA solution to prepare the bioink for stroma-rich model. In addition, BxPC-3 cells and NHDFs at the concentration of 3×10^6 cells/mL and 3×10^6 cells/mL (1:1), respectively, were mixed with GelMA solution to prepare the bioink for stroma-poor model. Before printing, the temperature of the receiving platform and printhead were set at 10°C and 15°C, respectively. The bioink was transferred to the printhead for a while until the

bioink reached the proper printing state. In this process, cell-laden beads were produced onto a hydrophobic membrane under the parameters of 0.1 MPa and 1400 ms. The center-to-center distance between GelMA hydrogel beads was fixed at 1000 μm by setting the coordinates of the hydrogel beads in G-code. As a result, an array of GelMA hydrogel beads around 800 μm was generated. Finally, the bioprinted cell-laden GelMA hydrogel beads were photo-crosslinked by 405 nm blue light (200 mW cm^{-2}) for 20 s before downstream culture.

2.6. Live/dead cell assay

Live/dead cell analysis was performed to assess cell viability of microtissues during the culture time at days 1, 4, and 7. Briefly, samples were stained with a live/dead viability kit (Beyotime, China) following the manufacturer's instructions. The samples were incubated at 37°C for 25 min, followed by a thorough wash in phosphate-buffered saline (PBS; Gibco, USA) and then observation under a fluorescence microscope (Nikon, Ti-U, Japan). Cell viability was determined according to the fluorescence area measured by ImageJ. Specifically, the fluorescent images of Calcein-AM and propidium iodide (PI) were respectively processed using ImageJ software, and transformed to grayscale for areas quantitation. Cell viability was calculated as the ratio of the area of Calcein-AM to the sum of area of Calcein-AM and PI.

2.7. Cell morphology analysis

To characterize the cell morphology and spatial distribution within the GelMA beads, F-actin staining on different PDAC microtissues was conducted at day 1, 4 and 7 of culture. Briefly, cell samples were washed using PBS, and then 4% paraformaldehyde (Beyotime, China) was used to fix cell for 4 h. Afterward, the samples were washed and stained with Alexa Fluor 488 phalloidin (1:200, Invitrogen, USA) for 2 h at room temperature. Finally, DAPI solution (1:1000, Biosharp, China) was added to stain cell nucleus for 10 min, which was observed using the fluorescence microscope after PBS washing for three times.

2.8. Immunofluorescence staining

To confirm the interactions between pancreatic cancer cells and normal fibroblasts, cytokeratin 19 (CK19) and smooth muscle actin-α (α-SMA) were used to stain BxPC-3 cells and NHDFs at days 1 and 7 of culture. Briefly, cell samples were gently washed with PBS, and then fixed with 4% paraformaldehyde for 4 h at room temperature. After that, samples were permeabilized by 0.25% (v/v) Triton X-100 (Beyotime, China) for 30 min on ice, and blocked with 5% (v/v) bovine serum albumin (BSA; Sigma-Aldrich, USA) solution for 1 h. Primary antibodies against α-SMA (1:100, Invitrogen, USA) and CK19 (1:50, Huabio, China) were added to samples and incubated overnight at 4°C. Subsequently, secondary antibodies including Alexa Flour 594 IgG and 488 IgG (1:200, Invitrogen, USA) were used to stain samples for 3 h at room temperature. Finally, DAPI solution (1:1000) was added for cell nucleus staining and incubated for 10 min. Samples were then fully washed with PBS and observed by fluorescence microscope.

2.9. Drug treatment

PDAC microtissues were cultured for 1 week before drug treatment. Gemcitabine powder (Sigma, USA) was separately dissolved in three concentrations of stock solution (50, 75 and 100 mM/mL). Then, the stock solution was diluted 1000 times in the culture medium and prepared into working fluids at different concentrations, including 50, 75 and 100 μM/mL. PDAC microtissues were cultured in the working fluids. Non-drug treatment PDAC microtissues were observed as control. After drug administration and incubation for 72 h, the PDAC microtissues were washed with PBS and then subject to cell viability analysis.

2.10. Statistical analysis

Experimental data from at least three independent experiments are expressed in mean ± standard error. Graphs were plotted using the GraphPad Prism 9 software and embellished using Inkscape. We further analyzed the significant differences of the data using two-way analysis of variance (ANOVA), and $P < 0.05$ was considered statistically significant.

3. Results

3.1. Printing of GelMA hydrogel beads and assessment of the microstructures

In this work, we aimed to produce GelMA beads to support pancreatic tumor-stroma microtissues, mainly considering that the spherical structure of beads allows full circulation of nutrients and oxygen[25,26]. Hence, GelMA beads at the concentration of 8% (w/v) were generated utilizing a pneumatic extrusion printhead. The printhead worked under pre-set G-code and printed hydrogel beads onto the substrate in a programmed intermittent pressure-driven mode. The intermittent pressure extrudes a low volume of GelMA hydrogel in a limited dispensing time, and round-shape beads are produced once the printhead is lifted up. The bioprinting system is shown in Figure 2A. It has been experimentally proven that the bioprinting system is well controllable and capable of producing uniform-sized GelMA hydrogel beads (Figure 2B). We can control the size of the formed GelMA hydrogel beads by adjusting the dispensing time in the G-code. As shown in Figure 2C, at a fixed pressure (0.1 MPa), GelMA hydrogel beads with

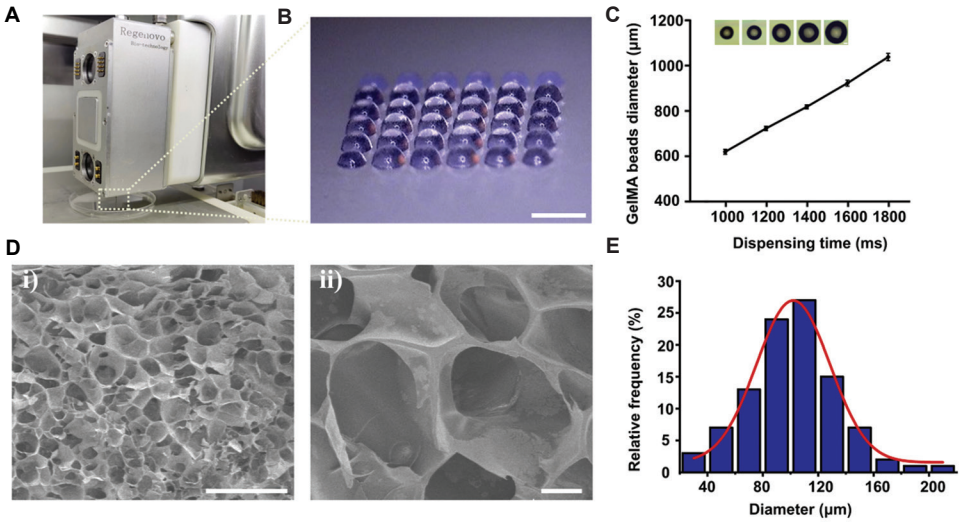

Figure 2. Bioprinting and microstructure characterization of GelMA beads. (A) Image of the bioprinting system. (B) Representative microscopic image showing the GelMA hydrogel beads array. Scale bar = 2 mm. (C) The average diameter of 8% (w/v) GelMA hydrogel beads as a function of dispensing time, with the air pressure of printing fixed at 0.1 MPa. Hydrogel beads at different diameter sizes were displayed within the diagram. Scale bar = 200 μm. (D) Scanning electron microscope images showing the section structure of 8% (w/v) GelMA hydrogel at different magnification. (i) Scale bar = 500 μm. (ii) Scale bar = 50 μm. (E) Pore size distribution of 8% (w/v) GelMA hydrogel.

an average diameter ranging from 620 to 1038 μm were produced according to the pre-set dispensing time from 1000 to 1800 ms, demonstrating the print controllability of the proposed bioprinting system.

We further performed SEM detection to observe the microstructures of the hydrogel beads. As illustrated in Figure 2D, the cross section of the GelMA hydrogel presented a porous honeycomb structure, suggesting that the hydrogel formed a crosslinked interpenetrating polymer network after photocuring. We further measured the pore size of the polymer network and found that most of the pore sizes of 8% (w/v) GelMA were in a range of around 100 – 120 μm (Figure 2E). This moderately sized porous structure can facilitate the entry of nutrients and the discharge of cell wastes, therefore providing appropriate microenvironment for cell growth and proliferation. The diffusion ability of the GelMA beads was further studied, as displayed in Figure S1. The FITC fluorescent molecules permeated through the GelMA beads increasingly during the immersion process, and achieved the overall diffusion within 20 min. The result, on the one hand, demonstrated the good permeability of the GelMA beads, and on the other hand, indicated that the hydrogel beads recapitulated the *in vivo* drug diffusion in a gradual fashion.

3.2. Printing of 3D PDAC microtissues

As reported, the *in vivo* PDAC is characterized by a mass of stroma component, and this contributes to its unique biological structure in which malignant cancer cells are embedded in a dense fibrous barrier[27,28]. This unique feature is a key factor affecting cancer progression and drug response[29]. To explore the effect of stroma content on drug treatment, we established 3D PDAC models with a tunable stromal microenvironment by modulating the density of stromal cells. Specifically, we mixed BxPC-3 cells and NHDFs at the ratio of 1:0 (mono-tumor microtissue), 1:1 (stroma-poor microtissue) and 1: 2 (stroma-rich microtissue) in GelMA solution for printing.

To measure cell viabilities within the GelMA hydrogel beads for different PDAC models, we selected different time points: day 1, day 4, and day 7 of culture to perform live/dead assay on different models. Representative fluorescent images are shown in Figure 3A. It was obvious that the cells embedded in the hydrogel beads proliferated and showed high cell viability. The pancreatic cancer cells formed spheroids under the support of hydrogel network, and the fibroblasts spread and wrapped the entire hydrogel bead after culturing 7 days. These results validate that the printed GelMA hydrogel beads are suitable for stable culture of both types of cells. We then quantified cell viabilities, with results presented in Figure 3B and Table S1, and found that the viability was higher than 90% for either model during 1-week culture. Notably, on day 1 after printing, the cells presented admirable viability, which highlights the cell-friendliness of our proposed bioprinting system for different cell types and cell densities. Interestingly, cell viability of the mono-tumor model was relatively higher compared to the co-culture model with stromal cell. Probably, this is because hydrogel beads with lower cell densities have sufficient growth space available for the embedded cells.

3.3. Stroma-tunable PDAC microtissues formation and characterization

To characterize cell morphology and spatial distribution of stromal cells in the stroma-tunable PDAC microtissues, we performed cytoskeleton staining for different models. As seen from Figure 4A, for the co-culture models (stroma-poor microtissue and stroma-rich microtissue), fibroblasts showed mostly round cell morphology at early stage of cell culture (day 1). However, with increasing days of culture, fibroblasts in the co-culture model became abundant in the hydrogel beads with distinct actin filaments. These findings suggest that we have simulated a suitable ECM environment (GelMA) for stromal cell maturation. More interestingly, the co-culture models both formed a fibroblastic network

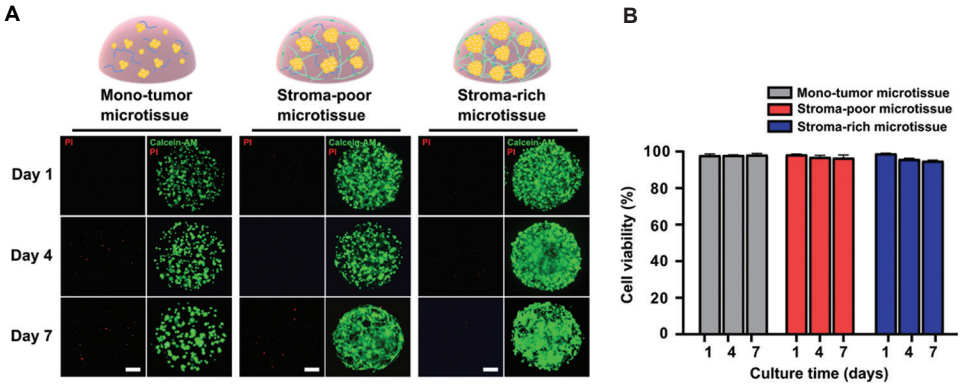

Figure 3. Cell viability analysis of the engineered three-dimensional pancreatic ductal adenocarcinoma (PDAC) models. (A) Representative fluorescent micrographs of three different PDAC models including mono-tumor, stroma-poor and stroma-rich microtissues at days 1, 4, and 7. Scale bar = 200 μm. (B) Cell viability. Experimental values are expressed in mean ± standard error, $n = 3$.

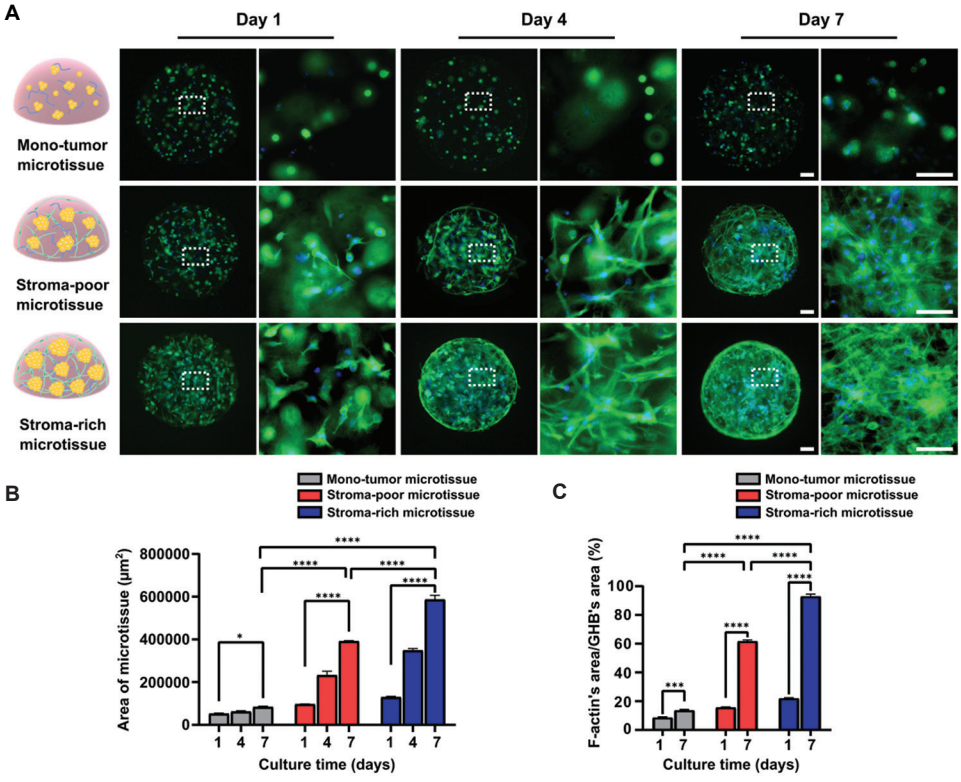

Figure 4. Morphology and organization of cells embedded in GelMA hydrogel beads of different pancreatic ductal adenocarcinoma (PDAC) models during 1-week culture. (A) F-actin staining of cell morphology and structure at day 1, 4 and 7. Green channel: F-actin. Blue channel: DAPI. Scale bar = 100 μm. (B) Assessment of the proliferation of different PDAC microtissues. (C) Assessment of the density of tumor microstructure. Experimental values are expressed in mean ± standard error, $n = 3$. Two-way ANOVA, $^{*}P < 0.05$, $^{***}P < 0.001$, $^{****}P < 0.0001$.

over 7 days of culture, and the pancreatic cancer cells were embedded in the fibroblastic network, confirming a dense stromal microenvironment created in the prepared PDAC microtissues.

To characterize cell proliferation of different pancreatic cancer models, we selected three time points: days 1, 4, and 7 of culture and calculated the changes in microtissue area in different models (Figure 4B). During the culture process, the area of tumor microtissue in different models increased due to spontaneous cell proliferation and aggregation. We also noticed that cells in the mono-culture PDAC model proliferated slowly, and the microtissue gained a mere 0.6-fold increase in area when cultured for 7 days. However, for both co-culture models, cell proliferation rates were significantly faster, especially for the stroma-rich PDAC model, and the area of microtissue was 3.5-fold higher than it was on day 1. The results showed that the fibroblasts in the cancer microenvironment promote tumor growth, and crosstalks between tumor and stroma may be involved.

To further evaluate the density of the produced PDAC microtissues, we calculated the ratio of the total cell area to the entire hydrogel bead area (Figure 4C). After 7 days of cultivation, the density of the mono-tumor microtissue was not significantly increased, with the percentage increasing from 8.6 ± 0.5% at the beginning (day 1) to 13.6 ± 0.7%. However, the ratio of total cell area to GelMA hydrogel bead area in the stroma-rich model was 21.9 ± 0.6% at day 1 of culture, and the model achieved a high density up to 92.8 ± 1.6% after culture for 1 week. The results verified that the cells in the stroma-rich model were more tightly connected to each other and formed a tight 3D fibroblastic network.

3.4. Imaging of tumor-stroma interactions in PDAC microtissues

After demonstrating the morphological and structural advantages of the printed 3D PDAC microtissues, we then tried to investigate the tumor-stoma crosstalk within the models based on specific markers immunostaining. As reported, α-SMA is the most common biomarker of CAFs[30,31]. We then evaluated α-SMA expression in co-culture models to explore whether the normal fibroblasts were activated over the co-culture period. Figure 5A showed that there were fewer α-SMA$^+$ cells in both co-culture models at day 1 of culture. However, the area of α-SMA$^+$ cells significantly increased when cultured for 7 days. Furthermore, the fibroblasts changed cellular morphology and acquired elongated spindle shapes. These features confirmed that NHDFs in both co-culture models were gradually activated and transformed to CAF-like phenotype through the interactions with pancreatic cancer cells[32]. For quantitative evaluation of α-SMA expression of stroma-rich and stroma-poor models, the area of α-SMA-derived fluorescent signal was calculated and is shown in Figure 5B. Obviously, after 7 days of culture, the areas of α-SMA$^+$ fibroblasts in stroma-poor and stroma-rich models were significantly increased, which were approximately 7- and 5.7-folds, respectively, larger than those at the beginning (day 1).

On the other hand, to distinguish cell types in the co-cultures and assess the amount of cancer cells, we stained cancer cells with CK19 (in red), considering that CK19 is positively expressed in pancreatic cancer cells[33]. We then measured the area of CK19$^+$ cells in three PDAC models at different time points (Figure 5C). As shown in the results, there was no significant difference in the area of CK19$^+$ cells in the three models at the early stage of culture (day 1). As co-culture period increased, we found that cancer cells in the stroma-rich model grew at the fastest rate when compared to the other two groups.

3.5. Drug response in different 3D PDAC models

Stromal cells in the pancreatic tumor microenvironment as well as the ECM are recognized as the important causes of increased tumor drug resistance[34-36]. Hence three different PDAC models including stoma-rich, stoma-poor, and mono-tumor microtissues were dealt with gemcitabine at different concentrations, a standardized drug for the treatment of pancreatic cancer[37]. Gemcitabine solutions of 50, 75, and 100 μM/mL were tested when three 3D PDAC microtissues have been cultured for 1 week. Meanwhile, three kinds of PDAC microtissues treated with non-drug medium and medium containing 0.1% dimethyl sulfoxide (DMSO) were, respectively, analyzed as controls. In this process, the produced PDAC microtissues were incubated with drug medium for 72 h before cell viability was determined. From the results (Figure 6A and Figure S2), three PDAC microtissues treated with non-drug medium and medium containing 0.1% DMSO displayed good cell states during the subsequent 72-h cultivation. While the mono-tumor microtissue showed poor resistance to drug and cell death occurred at a drug concentration of 50 μM/mL, the co-culture models demonstrated significant cell death when the concentration of drug increased up to 75 μM/mL. Notably, the dead cells in the mono-tumor microtissue were the larger cell spheroids within the hydrogel beads, indicating that the drug molecules diffused well in the GelMA hydrogel beads. While in both co-culture models, the dead cells were mainly distributed around the hydrogel beads, and this might be due to the fibrous barrier provided by the fibroblasts that prevents drug diffusion[38]. On the other hand, over the period of drug incubation, the 3D fibroblastic network involved in the co-culture models collapsed as the concentration of the drug increased.

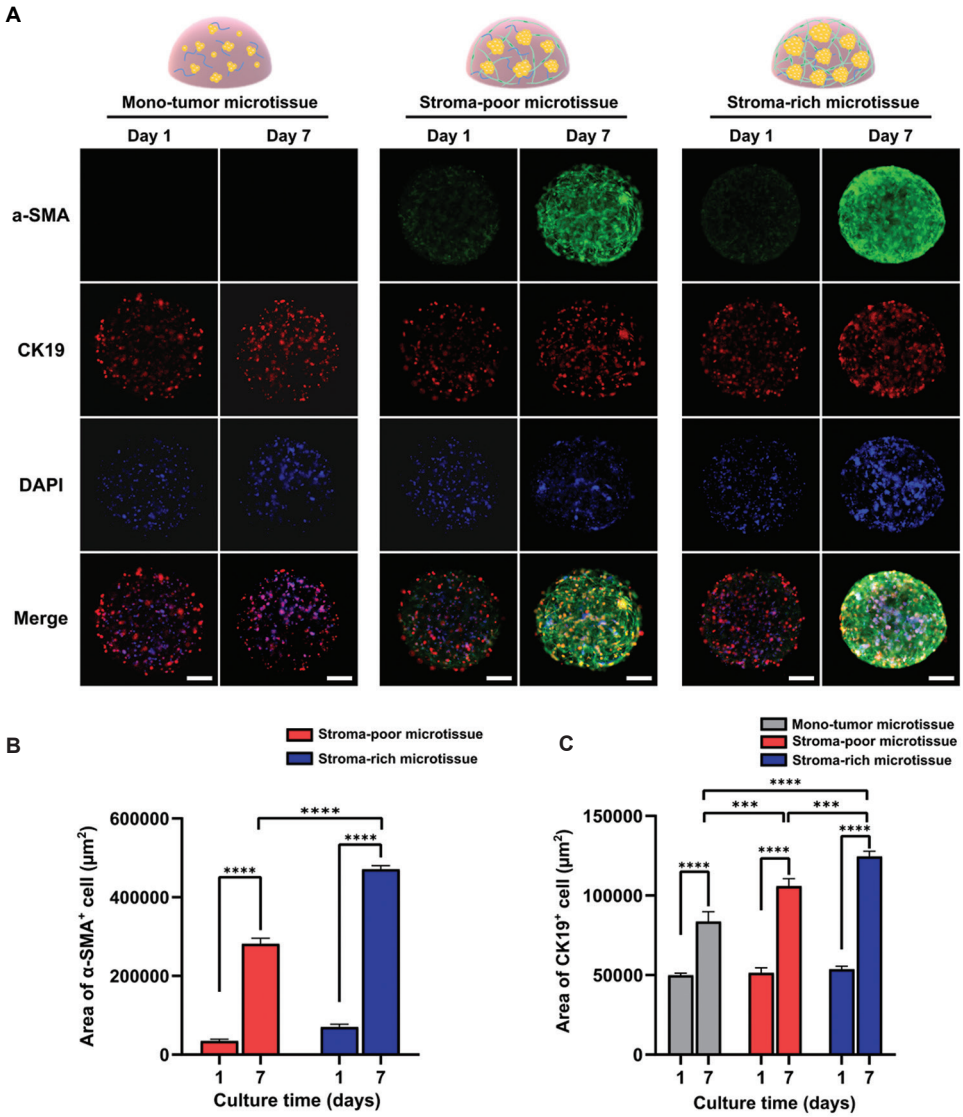

Figure 5. Tunable tumor-stroma microenvironment profiling. (A) Immunostaining of BxPC-3 cells and normal human dermal fibroblast cells with CK19 and α-SMA in different pancreatic ductal adenocarcinoma (PDAC) models at day 1, and 7. Green channel: α-SMA. Red channel: CK19. Blue channel: DAPI. Scale bar = 200 μm. (B) Quantitation of α-SMA expression in the co-culture models. (C) Quantitation of CK19 expression in different PDAC models. Experimental values are expressed in mean ± standard error, $n = 3$. Two-way ANOVA, $^{*}P < 0.05$, $^{**}P < 0.01$, $^{***}P < 0.001$, $^{****}P < 0.0001$.

To visualize the cell survival, we calculated the viability of all models (Figure 6B) and found that cell viabilities of the mono-culture PDAC model, stroma-poor PDAC model and stroma-rich PDAC model decreased in a gradient of increasing drug concentrations. At a drug concentration up to 100 μM/mL, there was 78.1 ± 2.9% of viable cells for the stroma-rich model, 70.1 ± 3.1% of viable cells for the stroma-poor model, and only 33.3 ± 3.5% of viable cells for the mono-culture model. Results demonstrated that the two co-culture models with stromal cell involvement had stronger drug resistance compared with the mono-culture model. A more visual heat map shown in Figure 6C shows that three PDAC models, including mono-tumor, stroma-poor and stroma-rich models, responded differently to the same drug concentration. The stroma-rich model was almost unaffected if the drug concentration was lower than 50 μM/mL. The cells in this model were slowly dying off when the drug concentration was higher than 50 μM/mL. These results confirmed that the fibrous barrier formed by CAFs prevented drug penetration into microtissues, and resulted in poor drug response[38].

4. Discussion

A lot of technologies for the fabrication of relevant PDAC microtissues have emerged in recent years, and these microtissues, including cell-rich spheroids and cell-laden

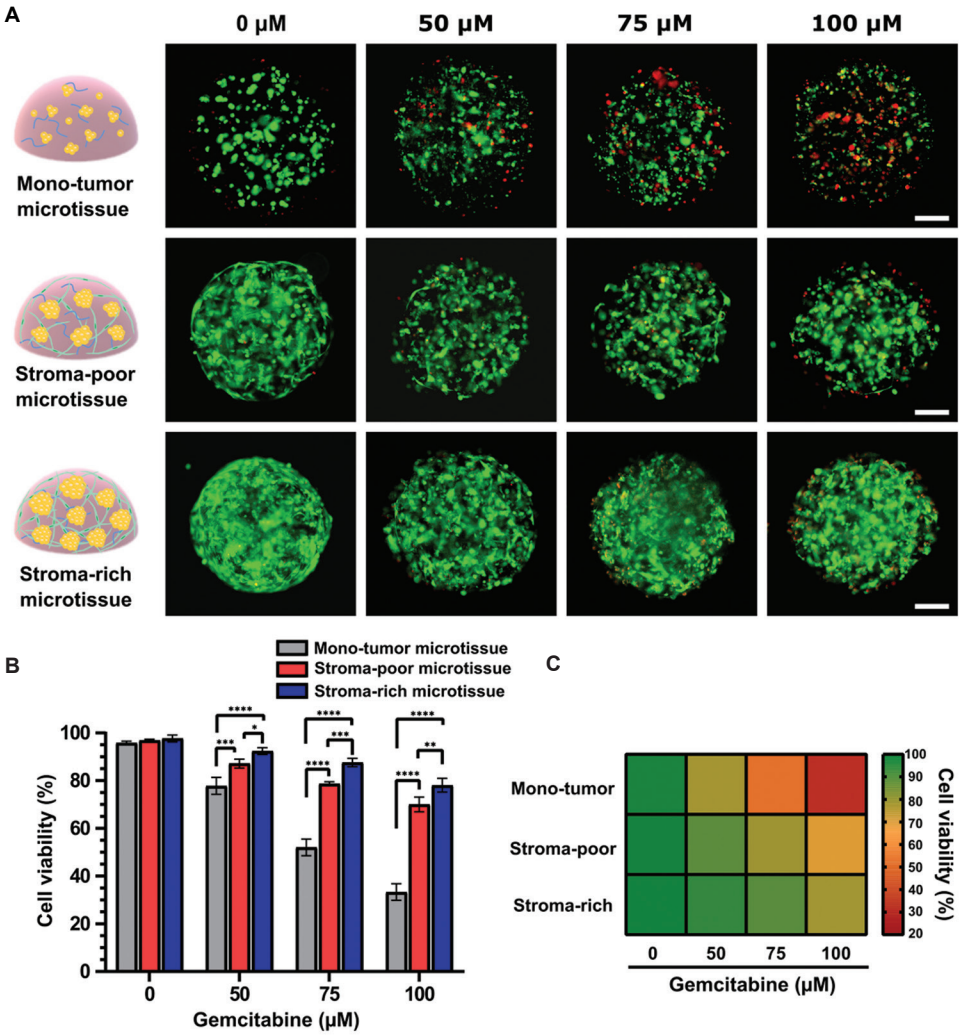

Figure 6. Drugs screening performed in different three-dimensional pancreatic ductal adenocarcinoma (PDAC) models after 7 days of culture. (A) Representative fluorescent micrographs of PDAC models after incubation with gemcitabine ranging from 50 to 100 μM/mL for 72 h. Non-drug-treated microtissues were observed as controls. Green channel: Calcein-AM. Red channel: PI. Scale bar = 200 μm. (B) Statistical plot of cell viabilities after treating PDAC models with different concentrations of gemcitabine for 72 h. (C) Heat map representing the drug treatment results. Experimental values are expressed in mean ± standard error, $n = 3$. Two-way ANOVA, $^{*}P < 0.05$, $^{**}P < 0.01$, $^{***}P < 0.001$, $^{****}P < 0.0001$.

hydrogel structures, serve as *in vitro* drug screening platforms[13], although they are still restrained by several limitations. Most cell-rich spheroids models mainly depend on ultra-low plate or hanging drop method[20,36], causing tedious operations. Besides, the produced cell spheroids often lack the biomimetic ECM components, which are considered one of the key elements in pancreatic cancer microenvironment[12]. Experiments employing certain cell-laden hydrogel PDAC models based on the animal-derived Matrigel matrix are prone to yield unrepeatable results due to the batch-to-batch properties of the material[39]. In view of the fact that a mass of collagen is present in the native PDAC ECM matrix, different cell-laden collagen models have been produced for use in pancreatic cancer research[21]. However, it is challenging to utilize some specific PDAC models *in vitro* due to their poor mechanical properties and slow crosslinking rate[12]. As an alternative, gelatin-based hydrogels, as a hydrolysate of collagen matrices, are used because they exhibit good performance in building 3D tumor models[40]. In particular, GelMA is a kind of gelatin-based hydrogel, which is synthesized by modifying gelatin with methacrylated groups. The modified material, which possesses the ability of rapid photocrosslinking and the tunable mechanical capacity, emerges as a popular ECM-mimetic hydrogel in tissue engineering[41].

In this work, we introduced a pancreatic cancer drug screening platform, which was made by utilizing a dot extrusion printing (DEP) system to print GelMA hydrogel

beads to support the co-culture of tumor cells and stromal fibroblasts. First, the proposed DEP system is different from the conventional continuous extrusion mode. Discrete hydrogel bead units could be printed with the pneumatic extrusion printhead under intermittent pressure-driven printing mode. We noticed that this kind of bioprinting system has the ability to print uniform-sized GelMA beads in an effective manner. Besides, the hydrogel beads were directly printed in gel state, which reduces GelMA droplets splashing and evaporation in the process of droplet-based bioprinting[42]. Therefore, the proposed DEP system has the potential to construct independent tumor microtissue array samples for large-scale drug testing.

GelMA material was applied to support the embedded cells. Several advantages of using GelMA include good printability, rapid crosslinking ability and remarkable biocompatibility[43]. SEM analysis further confirmed porous honeycomb structures within the 8% GelMA hydrogel, which have been proven to facilitate the diffusion of and culture medium and provide space for proliferating encapsulated cells[44-46]. Additionally, we printed GelMA hydrogel into microbead structure, which serves as microcarrier for cell growth. The hydrogel beads that encapsulate cells within a limited spherical structure (hundred microns in size) have been proved to promote the nutrient entry and waste removal[47]. To further verify the advantages of the microbead structure, we fabricated pancreatic cancer models including mono-tumor, stroma-poor and stroma-rich microtissues by culturing cells in a bulk GelMA hydrogel for 7 days. According to our results, cells encapsulated in the bulk hydrogel showed a poor proliferation status, especially in the central region of the bulk hydrogel, where cells proliferated more slowly when compared to cells in the surrounding region, and cell viability was lower than that of cells encapsulated in hydrogel beads after cultured for a week (Figure S3).

Through printing GelMA beads to encapsulate pancreatic cancer cells and stromal fibroblasts with tunable cell densities, we constructed 3D PDAC models with features of stroma-poor and stroma-rich fibroblastic networks. Further, we demonstrated that there were interactions between cancer cells and normal fibroblasts. Notably, while stromal cells within the PDAC model could be patient-derived PSCs, relevant report pointed out that PSCs isolated from patient specimens are at least partially activated and are not suitable for co-culture with pancreatic cancer cells aiming at exploring the process of normal fibroblasts induction to CAFs[48]. In our PDAC models, the normal fibroblasts changed their morphology when the CAF-relevant markers were expressed. On the other hand, we found that cancer cells proliferated with a rapid rate as the fibroblast density increased. Probably, this is because the abundant fibroblasts within the stroma-rich model secreted related factors that further promoted the tumor development, as many other works reported[49,50]. Future efforts should be concentrated at illustrating the detailed molecular mechanisms involved in the complex tumor-stoma interactions.

Finally, we demonstrated that the engineered PDAC microtissues with stromal barrier surrounding the cancer cells within GelMA beads could serve as a drug screening platform for *in vitro* prediction of chemotherapy efficacy. The printed PDAC microtissues are ECM-biomimetic, stroma-tunable, and resistant to chemotherapeutic drugs and can be used in in situ analysis. Here, our drug screening results showed that the formed PDAC microtissue with dense fibrous barrier was obviously resistant to gemcitabine. The engineered PDAC microtissue can be used to optimize novel treatment strategies, for example, combined therapy containing chemotherapeutic and stroma-targeted drugs, because of the stromal barrier formed. On the other hand, in addition to fibroblasts, other cellular components such as immune cells and endothelial cells are also vital for PDAC progression and drug resistance[51,52]. Therefore, we envision a more complicated microenvironment of our model by precise and controllable deposition of multiple cell types in the future.

5. Conclusion

Taken together, we engineered 3D pancreatic tumor-stroma ECM biophysical microtissues that recapitulate the key features of PDAC by utilizing the DEP system to print cell-laden GelMA hydrogel beads. The hydrogel beads provided a suitable ECM-mimetic environment that facilitates the growth of cells. A dense fibroblastic network with pancreatic cancer cells embedded was formed during 1-week co-culture, which recapitulates the desmoplastic PDAC structure *in vivo*. Importantly, the stroma-rich PDAC microtissue developed resistance to gemcitabine, which is typically observed in clinical practice, confirming the effect of stromal barrier on drug sensitivity. The proposed model is easy to construct and yields highly reproducible results, making it a valuable drug screening platform for rapid evaluation of cancer drug treatment and thereby narrowing the gap between drug development and clinical trials.

Acknowledgments

The authors acknowledge the SEM testing service from Zhejiang University.

Funding

This work was supported by the National Key Research and Development Program of China (2018YFA0109000)

and the National Natural Science Foundation of China (No. 31927801).

Conflict of interest

The authors declare no conflicts of interest.

Author contributions

Conceptualization: Xiaoyun Wei
Data curation: Beisi Huang
Formal analysis: Keke Chen
Investigation: Beisi Huang
Resources: Ling Wang
Supervision: Mingen Xu
Writing – original draft: Beisi Huang
Writing – review & editing: Xiaoyun Wei

Ethics approval and consent to participate

Not applicable.

Consent for publication

Not applicable.

Availability of data

Not applicable.

References

1. Makohon-Moore A, Iacobuzio-Donahue CA, 2016, Pancreatic cancer biology and genetics from an evolutionary perspective. *Nat Rev Cancer*, 16: 553–565.

   https://doi.org/10.1038/nrc.2016.66

2. Wolfgang CL, Herman JM, Laheru DA, *et al*., 2013, Recent progress in pancreatic cancer. *CA Cancer J Clin*, 63: 318–348.

   https://doi.org/10.3322/caac.21190

3. Siegel RL, Miller KD, Jemal A, 2018, Cancer statistics, 2018. *CA Cancer J Clin*, 68(1): 7–30.

   https://doi.org/10.3322/caac.21442

4. Stathis A, Moore MJ, 2010, Advanced pancreatic carcinoma: Current treatment and future challenges. *Nat Rev Clin Oncol*, 7: 163–172.

   https://doi.org/10.1038/nrclinonc.2009.236

5. Yang J, Xu R, Wang C, *et al*., 2021, Early screening and diagnosis strategies of pancreatic cancer: A comprehensive review. *Cancer Commun (Lond)*, 41: 1257–1274.

   https://doi.org/10.1002/cac2.12204

6. Heinrich MA, Mostafa AM, Morton JP, *et al*., 2021, Translating complexity and heterogeneity of pancreatic tumor: 3D *in vitro* to *in vivo* models. *Adv Drug Deliv Rev*, 174: 265–293.

   https://doi.org/10.1016/j.addr.2021.04.018

7. Ren B, Cui M, Yang G, *et al*., 2018, Tumor microenvironment participates in metastasis of pancreatic cancer. *Mol Cancer*, 17(1): 108.

   https://doi.org/10.1186/s12943-018-0858-1

8. Huang X, Ding L, Liu XK, *et al*., 2021, Regulation of tumor microenvironment for pancreatic cancer therapy. *Biomaterials*, 270: 120680.

   https://doi.org/10.1016/j.biomaterials.2021.120680

9. Uzunparmak B, Sahin IH, 2019, Pancreatic cancer microenvironment: A current dilemma. *Clin Transl Med*, 8: 2.

   https://doi.org/10.1186/s40169-019-0221-1

10. Wang S, Zheng Y, Yang F, *et al*., 2021, The molecular biology of pancreatic adenocarcinoma: Translational challenges and clinical perspectives. *Signal Transduct Target Ther*, 6(1): 249.

    https://doi.org/10.1038/s41392-021-00659-4

11. Valkenburg KC, De Groot AE, Pienta KJ, 2018, Targeting the tumour stroma to improve cancer therapy. *Nat Rev Clin Oncol*, 15: 366–381.

    https://doi.org/10.1038/s41571-018-0007-1

12. Monteiro MV, Ferreira LP, Rocha M, *et al*., 2022, Advances in bioengineering pancreatic tumor-stroma physiomimetic biomodels. *Biomaterials*, 287: 121653.

    https://doi.org/10.1016/j.biomaterials.2022.121653

13. Tomás-Bort E, Kieler M, Sharma S, *et al*., 2020, 3D approaches to model the tumor microenvironment of pancreatic cancer. *Theranostics*, 10(11): 5074–5089.

    https://doi.org/10.7150/thno.42441

14. Schnittert J, Bansal R, Prakash J, 2019, Targeting pancreatic stellate cells in cancer. *Trends Cancer*, 5: 128–142.

    https://doi.org/10.1016/j.trecan.2019.01.001

15. Thomas D, Radhakrishnan P, 2019, Tumor-stromal crosstalk in pancreatic cancer and tissue fibrosis. *Mol Cancer*, 18(1): 14.

    https://doi.org/10.1186/s12943-018-0927-5

16. Zhan HX, Zhou B, Cheng YG, *et al*., 2017, Crosstalk between stromal cells and cancer cells in pancreatic cancer: New insights into stromal biology. *Cancer Lett*, 392: 83–93.

    https://doi.org/10.1016/j.canlet.2017.01.041

17. Yang WG, Cai SX, Yuan Z, *et al*., 2019, Mask-free generation of multicellular 3D heterospheroids array for high-throughput combinatorial anti-cancer drug screening. *Mater Design*, 183: 108182.

    https://doi.org/10.1016/j.matdes.2019.108182

18. Zhuang P, Chiang YH, Fernanda MS, *et al*., 2021, Using spheroids as building blocks towards 3D bioprinting of tumor microenvironment. *Int J Bioprint*, 7: 444.

https://doi.org/10.18063/ijb.v7i4.444

19. Antunes J, Gaspar VM, Ferreira L, *et al*., 2019, In-air production of 3D co-culture tumor spheroid hydrogels for expedited drug screening. *Acta Biomater*, 94: 392–409.

https://doi.org/10.1016/j.actbio.2019.06.012

20. Monteiro MV, Gaspar VM, Mendes L, *et al*., 2021, Stratified 3D microtumors as organotypic testing platforms for screening pancreatic cancer therapies. *Small Methods*, 5: 2001207.

https://doi.org/10.1002/smtd.202001207

21. Monteiro MV, Rocha M, Gaspar VM, *et al*., 2022, Programmable living units for emulating pancreatic tumor-stroma interplay. *Adv Healthc Mater*, 11: e2102574.

https://doi.org/10.1002/adhm.202102574

22. Murphy SV, De Coppi P, Atala A, 2020, Opportunities and challenges of translational 3D bioprinting. *Nat Biomed Eng*, 4: 370–80.

https://doi.org/10.1038/s41551-019-0471-7

23. Ayan B, Heo DN, Zhang Z, *et al*., 2020, Aspiration-assisted bioprinting for precise positioning of biologics. *Sci Adv*, 6: eaaw5111.

https://doi.org/10.1126/sciadv.aaw5111

24. Matai I, Kaur G, Seyedsalehi A, *et al*., 2020, Progress in 3D bioprinting technology for tissue/organ regenerative engineering. *Biomaterials*, 226: 119536.

https://doi.org/10.1016/j.biomaterials.2019.119536

25. Xie MJ, Gao Q, Zhao HM, *et al*., 2019, Electro-assisted bioprinting of low-concentration GelMA microdroplets. *Small*, 15: 1804216.

https://doi.org/10.1002/smll.201804216

26. Clua-Ferré L, De Chiara F, Rodríguez-Comas J, *et al*., 2022, Collagen-tannic acid spheroids for β-cell encapsulation fabricated using a 3D bioprinter. *Adv Mater Technol-US*, 7: 2101696.

https://doi.org/10.1002/admt.202101696

27. Vennin C, Murphy KJ, Morton JP, *et al*., 2018, Reshaping the tumor stroma for treatment of pancreatic cancer. *Gastroenterology*, 154: 820–838.

https://doi.org/10.1053/j.gastro.2017.11.280

28. Rubiano A, Delitto D, Han S, *et al*., 2018, Viscoelastic properties of human pancreatic tumors and *in vitro* constructs to mimic mechanical properties. *Acta Biomater*, 67: 331–340.

https://doi.org/10.1016/j.actbio.2017.11.037

29. Looi CK, Chung FF, Leong CO, *et al*., 2019, Therapeutic challenges and current immunomodulatory strategies in targeting the immunosuppressive pancreatic tumor microenvironment. *J Exp Clin Canc Res*, 38: 162.

https://doi.org/10.1186/s13046-019-1153-8

30. Rimal R, Desai P, Daware R, *et al*., 2022, Cancer-associated fibroblasts: Origin, function, imaging, and therapeutic targeting. *Adv Drug Deliv Rev*, 189: 114504.

https://doi.org/10.1016/j.addr.2022.114504

31. Han CC, Liu TY, Yin R, 2020, Biomarkers for cancer-associated fibroblasts. *Biomark Res*, 8: 64.

https://doi.org/10.1186/s40364-020-00245-w

32. Lee JH, Kim SK, Khawar IA, *et al*., 2018, Microfluidic co-culture of pancreatic tumor spheroids with stellate cells as a novel 3D model for investigation of stroma-mediated cell motility and drug resistance. *J Exp Clin Canc Res*, 37: 4.

https://doi.org/10.1186/s13046-017-0654-6

33. Mehrpouya M, Pourhashem Z, Yardehnavi N, *et al*., 2019, Evaluation of cytokeratin 19 as a prognostic tumoral and metastatic marker with focus on improved detection methods. *J Cell Physiol*, 234: 21425–21435.

https://doi.org/10.1002/jcp.28768

34. Von Ahrens D, Bhagat TD, Nagrath D, *et al*., 2017, The role of stromal cancer-associated fibroblasts in pancreatic cancer. *J Hematol Oncol*, 10: 76.

https://doi.org/10.1186/s13045-017-0448-5

35. Ligorio M, Sil S, Malagon-Lopez J, *et al*., 2019, Stromal microenvironment shapes the intratumoral architecture of pancreatic cancer. *Cell*, 178: 160–175.

https://doi.org/10.1016/j.cell.2019.05.012

36. Ware MJ, Keshishian V, Law JJ, *et al*., 2016, Generation of an *in vitro* 3D PDAC stroma rich spheroid model. *Biomaterials*, 108: 129–142.

https://doi.org/10.1016/j.biomaterials.2016.08.041

37. Berlin J, Benson AB 3rd, 2010, Gemcitabine remains the standard of care for pancreatic cancer. *Nat Rev Clin Oncol*, 7: 135–137.

https://doi.org/10.1038/nrclinonc.2010.16

38. Liu HQ, Shi Y, Qian F, 2021, Opportunities and delusions regarding drug delivery targeting pancreatic cancer-associated fibroblasts. *Adv Drug Deliv Rev*, 172: 37–51.

https://doi.org/10.1016/j.addr.2021.02.012

39. Benton G, Arnaoutova I, George J, *et al*., 2014, Matrigel: From discovery and ECM mimicry to assays and models for cancer research. *Adv Drug Deliv Rev*, 79-80: 3–18.

https://doi.org/10.1016/j.addr.2014.06.005

40. Liu HY, Korc M, Lin CC, 2018, Biomimetic and enzyme-responsive dynamic hydrogels for studying cell-matrix interactions in pancreatic ductal adenocarcinoma. *Biomaterials*, 160: 24–36.

https://doi.org/10.1016/j.biomaterials.2018.01.012

41. Ying GL, Jiang N, Yu CJ, *et al*., 2018, Three-dimensional bioprinting of gelatin methacryloyl (GelMA). *Biodes Manuf*, 1: 215–224.

https://doi.org/10.1007/s42242-018-0028-8

42. Gudapati H, Dey M, Ozbolat I, 2016, A comprehensive review on droplet-based bioprinting: Past, present and future. *Biomaterials*, 102: 20–42.

https://doi.org/10.1016/j.biomaterials.2016.06.012

43. Miri AK, Hosseinabadi HG, Cecen B, *et al*., 2018, Permeability mapping of gelatin methacryloyl hydrogels. *Acta Biomater*, 77: 38–47.

https://doi.org/10.1016/j.actbio.2018.07.006

44. Zhou MM, Lee BH, Tan LP, 2017, A dual crosslinking strategy to tailor rheological properties of gelatin methacryloyl. *Int J Bioprint*, 3(2): 130–137.

https://doi.org/10.18063/IJB.2017.02.003

45. Xu P, Guan J, Chen Y, *et al*., 2021, Stiffness of photocrosslinkable gelatin hydrogel influences nucleus pulposus cell properties *in vitro*. *J Cell Mol Med*, 25: 880–991.

https://doi.org/10.1111/jcmm.16141

46. Yang Y, Xu R, Wang C, *et al*., 2022, Recombinant human collagen-based bioinks for the 3D bioprinting of full-thickness human skin equivalent. *Int J Bioprint*, 8: 611.

http://doi.org/10.18063/ijb.v8i4.611

47. Yang T, Zhang QY, Xie L, *et al*., 2021, hDPSC-laden GelMA microspheres fabricated using electrostatic microdroplet method for endodontic regeneration. *Mater Sci Eng C Mater Biol Appl*, 121: 111850.

https://doi.org/10.1016/j.msec.2020.111850

48. Tanaka HY, Kurihara T, Nakazawa T, *et al*., 2020, Heterotypic 3D pancreatic cancer model with tunable proportion of fibrotic elements. *Biomaterials*, 251: 120077.

https://doi.org/10.1016/j.biomaterials.2020.120077

49. Wu FL, Yang J, Liu J, *et al*., 2021, Signaling pathways in cancer-associated fibroblasts and targeted therapy for cancer. *Signal Transduct Target Ther*, 6: 218.

https://doi.org/10.1038/s41392-021-00641-0

50. Boyd LN, Andini KD, Peters GJ, *et al*., 2022, Heterogeneity and plasticity of cancer-associated fibroblasts in the pancreatic tumor microenvironment. *Semin Cancer Biol*, 82: 184–196.

https://doi.org/10.1016/j.semcancer.2021.03.006

51. Yang J, Li YZ, Sun ZW, *et al*., 2021, Macrophages in pancreatic cancer: An immunometabolic perspective. *Cancer Lett*, 498: 188–200.

https://doi.org/10.1016/j.canlet.2020.10.029

52. Nielsen MF, Mortensen MB, Detlefsen S, 2016, Key players in pancreatic cancer-stroma interaction: Cancer-associated fibroblasts, endothelial and inflammatory cells. *World J Gastroenterol*, 22: 2678–2700.

https://doi.org/10.3748/wjg.v22.i9.2678